



Experimental Measurements and Modeling of Vapor–Liquid Equilibria for Eight Mixtures Containing trans -1-Chloro-3,3,3-trifluoropropene (R1233zd(E)) and 2-Chloro-3,3,3-trifluoropropene (R1233xf)

Jamal El Abbadi, Julien Brocuse, Alain Valtz, Christophe Coquelet, Houriez Céline

► To cite this version:

Jamal El Abbadi, Julien Brocuse, Alain Valtz, Christophe Coquelet, Houriez Céline. Experimental Measurements and Modeling of Vapor–Liquid Equilibria for Eight Mixtures Containing trans -1-Chloro-3,3,3-trifluoropropene (R1233zd(E)) and 2-Chloro-3,3,3-trifluoropropene (R1233xf). Journal of Chemical and Engineering Data, 2023, 68 (9), pp.2316-2331. 10.1021/acs.jced.3c00296 . hal-04197103

HAL Id: hal-04197103

<https://hal.science/hal-04197103>

Submitted on 5 Sep 2023

HAL is a multi-disciplinary open access archive for the deposit and dissemination of scientific research documents, whether they are published or not. The documents may come from teaching and research institutions in France or abroad, or from public or private research centers.

L'archive ouverte pluridisciplinaire **HAL**, est destinée au dépôt et à la diffusion de documents scientifiques de niveau recherche, publiés ou non, émanant des établissements d'enseignement et de recherche français ou étrangers, des laboratoires publics ou privés.

Experimental measurements and modelling of vapor-liquid equilibria for eight mixtures containing trans-1-chloro-3,3,3-trifluoropropene (R1233zd(E)) and 2-chloro-3,3,3-trifluoropropene (R1233xf)

Jamal El Abbadi^a, Julien Brocuse^b, Alain Valtz^a, Christophe Coquelet^{a,b*}, Céline Houriez^a

^aMines Paris, PSL University, Centre for Thermodynamics of Processes (CTP), 77300 Fontainebleau, France

^bUniversité de Toulouse, IMT Mines Albi, UMR CNRS 5302, Centre RAPSODEE, Campus Jarlard, 81013 Albi, CT Cedex 9, France

*Corresponding author: christophe.coquelet@mines-albi.fr

Abstract

Isothermal vapor-liquid equilibria (VLE) for eight binary systems involving R1233zd(E) (R1233zd(E)+Butane, R1233zd(E)+CO₂, R1233zd(E)+HCl, R1233zd(E)+R134a, R1233zd(E)+R152a, R1233zd(E)+R245fa) and R1233xf (R1233xf+R134a, R1233xf+R152a, R1233xf+R245fa) were measured at temperatures from 263 to 353 K. The experiments were conducted by means of a static analytic apparatus with phase analysis via gas chromatography, with resulting maximum expanded uncertainties of 0.2 K for temperatures, 10 kPa for pressure and 0.04 for vapor and liquid mole fractions. The main advantage of the equipment is that vapor and liquid samples are taken from vapor and liquid phase by two capillary samplers (ROLSI®). The Peng-Robinson equation of state and a modified Patel-Teja equation of state are both considered to represent the experimental data. If possible, comparison between the new experimental data and prediction with REFPROP 10.0 software are realized.

Keywords: Working fluids, Hydrofluoro-olefins, Hydrofluorocarbons, vapor-liquid equilibrium, modeling.

Symbols and abbreviations

AAD: Average Absolute Deviation

ASHRAE: American Society of Heating, Refrigerating and Air-Conditioning Engineers

CAS: Chemical Abstracts Services

GC: Gas chromatography

GUM: Guide for Uncertainty Measurements

GWP: Global Warming Potential

HCFO: Hydrochlorofluoroolefin

HFC: Hydrofluorocarbon

HFO: Hydrofluoroolefin

HP: Heat pump

HVAC: Heating, Ventilation and Air conditioning

MC: Mathias-Copeman

MM: Molecular Mass

NEoS: New Equation of State

ORC: Organic Rankine Cycle

PR: Peng-Robinson

ROLSI: Rapid On-Line Sampler Injector

TCD: Thermal Conductivity Detector

vdW: van der Waals

VLE: Vapor-liquid equilibrium

Symbols

a: Energetic parameter of the cubic equation of state

b: Co-volume

c: Third parameter of the cubic equation of state

F: Function

k: Binary interaction parameter

m: Parameter of the Mathias-Copeman alpha-function

N: Number of points

P: Pressure

R: Universal Constant for Ideal Gas (taken as $8.3144598 \text{ J.mol}^{-1}.\text{K}^{-1}$)

T: Temperature

v: Molar volume

x: Liquid fraction

y: Vapor fraction

z: Global fraction

Z: Compressibility factor

Greek letters

α : Temperature dependent part of the energetic parameter in the cubic equation of state

α_{12} : Relative volatility of component 1 relative to component 2

σ : Standard deviation

Ω : Parameter of the cubic equation of state

ω : Acentric factor

Subscripts

c: Critical parameter

cal: Calculated property

exp: Experimental property

i: i-th component

j: j-th component

L: Liquid property

obj: Objective

opt: Optimized

Superscript

1. Introduction

HVAC systems and especially Organic Rankine Cycles (ORCs), Heat Pumps (HPs) and Kalina Cycles are a major part of the ongoing investigation and investment to valorize low grade industrial waste heat^{1,2,3}.

Since F-gas regulations⁴, and Kigali and Kyoto protocols before that, HFCs are being replaced by low GWP alternatives, namely HFOs refrigerants. Considering pure refrigerants, the list of promising candidates is reduced as the constraints increases, whether it is environmental, thermodynamical, economical, security ones or others. A handful is then considered by most of the scientific community for investigations⁵.

Zeotropic mixtures of refrigerant can be a great solution. First, the glide inherent of zeotropic mixtures allows to better fit the temperature of the heat source, reducing exergetic losses and increasing efficiency⁶, especially at low temperatures^{7,8}. Second, mixing low GWP refrigerant with their high performances HFCs predecessor allows to find a common middle ground resulting in similar performances with low GWP. Mixtures can be a way to mitigate the undesirable properties of pure refrigerants and allows for a bigger list of refrigerants to be considered, in combination with others.

R1234yf is the main candidate for the replacement of R134a in HVAC applications⁹, while R1233zd(E) is mainly investigated to replace R245fa¹⁰ in ORCs^{11,12} and HPs¹³.

Thermophysical properties data are essential for the selection of the best working fluid. In particular, adequate equipment are needed for the measurement and identification of the phase diagram¹⁴.

Previous research provided isothermal vapor-liquid equilibria (VLE) data for different mixtures with R1234yf¹⁵⁻¹⁸. This paper focuses on the isothermal VLE data of mixtures with R1233zd(E) and R1233xf, a refrigerant which constitutes one of the main building blocks in the synthesis of R1234yf¹⁹. HCl + R1233zd(E) mixture is also included in the measurements. While it is not a refrigerant mixture, HCl can be found after the synthesis of R1233zd(E) as impurity. It is therefore useful to plot this mixture's phase diagram in order to properly separate them.

Vapor pressure of R1233zd(E) have been measured by several laboratories^{20,21,22}. VLE mixture data involving R1233zd(E) found in the open literature concern R1233zd(E)+HC-600a²³ and R1233zd(E)+R1234yf¹⁵ systems.

The only data found in the open literature on R1233xf concern pure vapor pressure measurement²⁴ and VLE data of the mixtures R1234yf+R1233xf^{15,25} and R1233xf+HCFC-244bb²⁵. Measurements of R1233xf saturation liquid density are provided in the supporting information, Table S. 1.

Hence, we provide in this work isothermal vapor-liquid equilibria (VLE) data of different HCFO/HFC mixtures obtained with a static-analytic method. We then correlate the data with the Peng-Robinson equation of state²⁶ (PR) and a modified Patel-Teja cubic equation of state (NEoS²⁷), both associated with a Mathias-Copeman alpha function²⁸ and classical van der Waals mixing rules.

2. Experimental

2.1 Materials. The five refrigerants and three natural products used for the vapor-liquid equilibrium (VLE) measurements are listed in Table 1, along with the details about their ASHRAE denomination, chemical formula, CAS number, name of the supplier and the product purity indicated by the supplier and verified by GC. No further purification of the chemical products was needed. Degassing was performed when loading the chemicals into the equilibrium cell.

Table 1: Chemical sample: Refrigerants used for the experimental measurements with supplier and purities.

Compounds	ASHRAE name	Formula	CAS number	Supplier	Purity* % vol.
n-Butane	R600	C ₄ H ₁₀	106-97-8	Sigma-Aldrich	99.95
Hydrogen chloride	/	HCl	7647-01-0	Alpha gaz	99.8
Carbon dioxide	R744	CO ₂	124-38-9	Air liquide	>99.995
1,1,1,2-tetrafluoroethane	R134a	C ₂ H ₂ F ₄	811-97-2	Climalife	>99
1,1-difluoroethane	R152a	C ₂ H ₄ F ₂	75-37-6	Dehon	>99
1,1,1,3,3-pentafluoropropane	R245fa	C ₃ H ₃ F ₅	460-73-1	Honeywell	>99
Trans-1-chloro-3,3,3-trifluoropropene	R1233zd(E)	C ₃ H ₂ F ₃ Cl	102687-65-0	Synquest	>97
2-chloro-3,3,3-trifluoropropene	R1233xf	C ₃ H ₂ F ₃ Cl	2730-62-3	Synquest	>99

*: Checked with Gas Chromatograph

2.2 Experimental apparatus. The equipment used for the VLE measurements is based in a static-analytic method with liquid and vapor phase sampling using capillary samplers ROLSI®²⁹. The equipment can be categorized under « Analytical technique with sampling, isothermal AnT » according to the Dohrn et al. classification³⁰.

The equipment is identical to the one used in previous similar measurements^{15,16,31–33}. Validation of the experimental setup can be found in previous publications^{16,32}. The main part of the apparatus is the equilibrium cell, where the two-phase equilibrium takes place. The flow diagram of the apparatus is displayed in Figure 1.

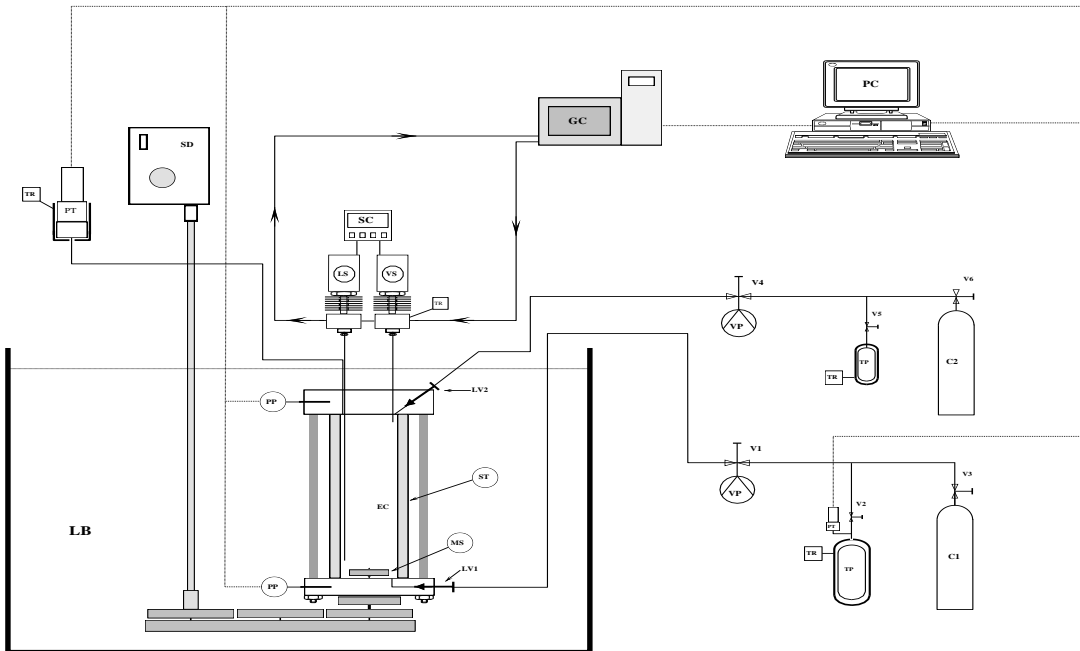


Figure 1 : Flow diagram of the static-analytic apparatus. C1 : more volatile compound ; C2 : less volatile compound ; EC : equilibrium cell ; GC : gas chromatograph ; LB : liquid bath ; LS : liquid sampler ; LV : loading valve ; MS : magnetic stirrer ; PC : personal computer ; PP : platinum resistance thermometer probe ; PT : pressure transducer ; SD : stirring device ; SC : sample controlling ; ST : sapphire tube ; TP : thermal press ; TR : temperature regulator ; V : valve ; VP : vacuum pump ; VS : vapor sampler. Reproduced from Juntarachat et al, 2014¹⁶, Copyright (2023) with permission from Elsevier.

The apparatus is equipped with a thermo-regulated liquid bath where the equilibrium cell is immersed. The bath ensures the control of the temperature within 0.01 K.

The temperature measurements inside the equilibrium cell are performed using two platinum resistance thermometer probes (Pt100), inserted into the top and bottom flanges of the equilibrium cell. During measurements, the temperature difference between these two probes was lower than the uncertainty of measurement. Two additional temperature probes are used to control the temperature inside the thermal press used to load the chemical products into the equilibrium cell.

The Pt100 probes are connected to a data acquisition unit (HP34970A). The Pt100 probes are calibrated against a 25 Ω reference platinum resistance thermometer (Pt25 – Hart Scientific). The Pt25 reference probe was calibrated by the “Laboratoire National d’Essais de Paris” based on the 1990 International Temperature Scale (ITS 90). The temperature accuracy is estimated to be within ± 0.03 K.

The pressure is measured using one of the two pressure transducers (Druck, 0-3 MPa, 0-30 MPa) installed on the apparatus. The choice of pressure transducer is dependent upon the maximum pressures generated by the system studied. The two pressure transducers are also connected to the data acquisition unit. The pressure transducers were calibrated against a pressure automated calibrator (GE Sensing, model PACE 5000). The pressure accuracy of the transducers is estimated to be within \pm 0.0004 MPa. Type B uncertainties³⁴ were considered for the determination of temperature and pressure uncertainties.

The molar compositions of the phases in the cell are determined after analysis of liquid and vapor samples by a gas chromatograph (PERICHROM, model PR2100) equipped with a thermal conductivity detector (TCD). The analytical column within the gas chromatograph is a RESTEK, 1% RT-1000 on Carboblack B, 60/80 mesh (length: 2.4m, diameter: 2mm from RESTEK, ID Silcosteel).

The TCD is calibrated by introducing manually known amounts of each pure compound (for the system studied) into the injector of the gas chromatograph, using an automatic syringe. The calibration equation was fitted to relate the response of the TCD to the amount of the component introduced. The relative accuracy for each mole number is given in Table 2.

Table 2 : Mole number relative accuracy (in %) of TCD for each component in each system.

Binary system	Component 1	Component 2
Butane + R1233zd(E)	1.0	1.8
HCl + R1233zd(E)	1.4	2.0
CO ₂ + R1233zd(E)	1.2	2.5
R134a + R1233zd(E)	2.4	2.0
R152a + R1233zd(E)	0.9	2.5
R245fa + R1233zd(E)	0.6	2.0
R134a + R1233xf	0.9	0.7
R245fa + R1233xf	0.5	0.6

The determination of the uncertainty of the mole³⁵ takes into account the repeatability of the measurement (type A according to the GUM), the calibration of the TCD and the purity of the chemicals. The molar fraction is determined from the number of moles of each compound in the analyzed sample, given by $x_1 = \frac{n_1}{n_1+n_2}$ for the liquid phase. Detailed calculations of the uncertainties are provided in the Supporting information.

2.3 Experimental procedure. At ambient temperature, the equilibrium cell and its loading lines are made under vacuum. A first thermal press is loaded with one of the compounds, the second press with the other compound. The liquid bath is set to the desired temperature. When the equilibrium temperature is reached (the equilibrium temperature is reached when the Pt100 probes give the same temperature value within their temperature uncertainty for at least 10 minutes), an amount of about 5 cm³ of the less volatile component is introduced into the equilibrium cell. Its vapor pressure is then measured at the equilibrium temperature.

Then, given amount of the second component (the more volatil) are introduced in successive steps, leading to equilibrium with different composition mixtures in order to have sufficient data points to cover the two-phase envelope.

The equilibrium inside the cell is assumed to be reached when the pressure is stable for at least 10 minutes within ± 0.001 MPa under continuous stirring.

For each equilibrium condition, six or more samples of both vapor and liquid phases are taken using the capillary sampler ROLSI®.³⁶ (Armines' patent FR 2853414) and analyzed in order to verify the repeatability of the measurements, as to have a standard deviation less than 1%.

3. Experimental measurements

The VLE measurements of the eight binary mixtures have been carried out in this work, considering two isotherms for each mixture (three in the case of two of those mixtures). Results from measurement and modeling are compiled in Tables 3 to 10 with expanded uncertainties for temperature, pressure and molar fractions at the bottom of each table. *P-x,y* phase diagrams are provided in Figures 2 to 9. Relative volatilities and K-values are provided in the supplementary materials.

The binary systems studied are n-Butane + R1233zd(E) (Figure 2), HCl + R1233zd(E) (Figure 3), CO₂ + R1233zd(E) (Figure 4), R134a + R1233zd(E) (Figure 5), R152a + R1233zd(E) (Figure 6), R245fa + R1233zd(E) (Figure 7), R134a + R1233xf (Figure 8) and R245fa + R1233xf (Figure 9).

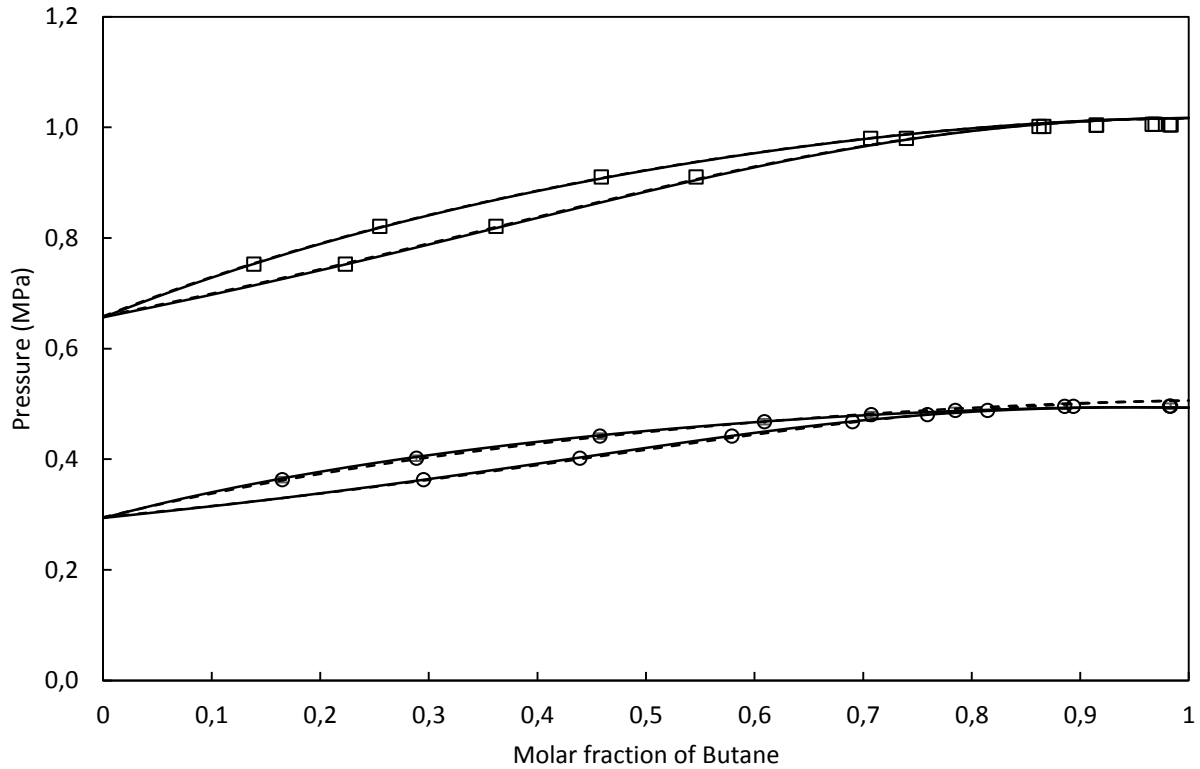


Figure 2 : P-xy phase diagram of n-Butane – R1233zd(E) binary system. Experimental values: 323.27 K (○) and 353.23 K (□). Modelling results: Peng-Robinson (Solid lines), NEoS (Dashed lines).

Table 3 : Experimental and modeling vapor-liquid equilibria of n-Butane(1) + R1233zd(E)(2) at temperature T, liquid composition x, gas composition y, and pressure P for a number of samples n, and associated standard deviation of composition σ

Experimental				NEoS				Peng-Robinson			
P	n	x ₁	σ _{x1}	n	y ₁	σ _{y1}	P _{calc}	y _{1,calc}	P _{calc}	y _{1,calc}	
MPa										MPa	MPa
T = 323.27 K											
0.3631	6	0.165	0.0001	7	0.295	0.004	0.3667	0.3031	0.3652	0.3039	
0.4019	7	0.288	0.0004	8	0.439	0.002	0.4054	0.4409	0.4040	0.4427	
0.4419	15	0.458	0.0006	9	0.579	0.005	0.4438	0.5802	0.4430	0.5830	

0.4679	6	0.609	0.0002	7	0.690	0.0009	0.4679	0.6859	0.4679	0.6893
0.4807	4	0.707	0.0002	4	0.759	0.0009	0.4792	0.7535	0.4798	0.7570
0.4883	6	0.785	0.0004	5	0.814	0.0004	0.4855	0.8094	0.4868	0.8127
0.4957	8	0.886	0.0002	5	0.894	0.0002	0.4901	0.8899	0.4924	0.8922
0.4960	8	0.983	0.0002	8	0.982	0.0001	0.4896	0.9820	0.4932	0.9825

T = 353.23 K

0.7528	7	0.139	0.0002	6	0.223	0.002	0.7528	0.2227	0.7529	0.2249
0.8211	4	0.255	0.0003	4	0.362	0.0006	0.8183	0.3614	0.8183	0.3631
0.9104	7	0.459	0.0009	5	0.546	0.001	0.9093	0.5531	0.9074	0.5526
0.9802	8	0.707	0.0002	6	0.740	0.0007	0.9866	0.7512	0.9802	0.7486
1.0018	7	0.862	0.0003	6	0.866	0.0008	1.0176	0.8764	1.0072	0.8741
1.0040	10	0.914	0.0003	6	0.915	0.0007	1.0248	0.9216	1.0128	0.9198
1.0057	5	0.969	0.0003	5	0.966	0.0005	1.0302	0.9706	1.0163	0.9698
1.0046	9	0.984	0.0002	7	0.982	0.0003	1.0313	0.9843	1.0168	0.9839

U(T, k=2) = 0.2 K, U(P, k=2) = 0.004 MPa, U(x₁,y₁,k=2) = 0.04.

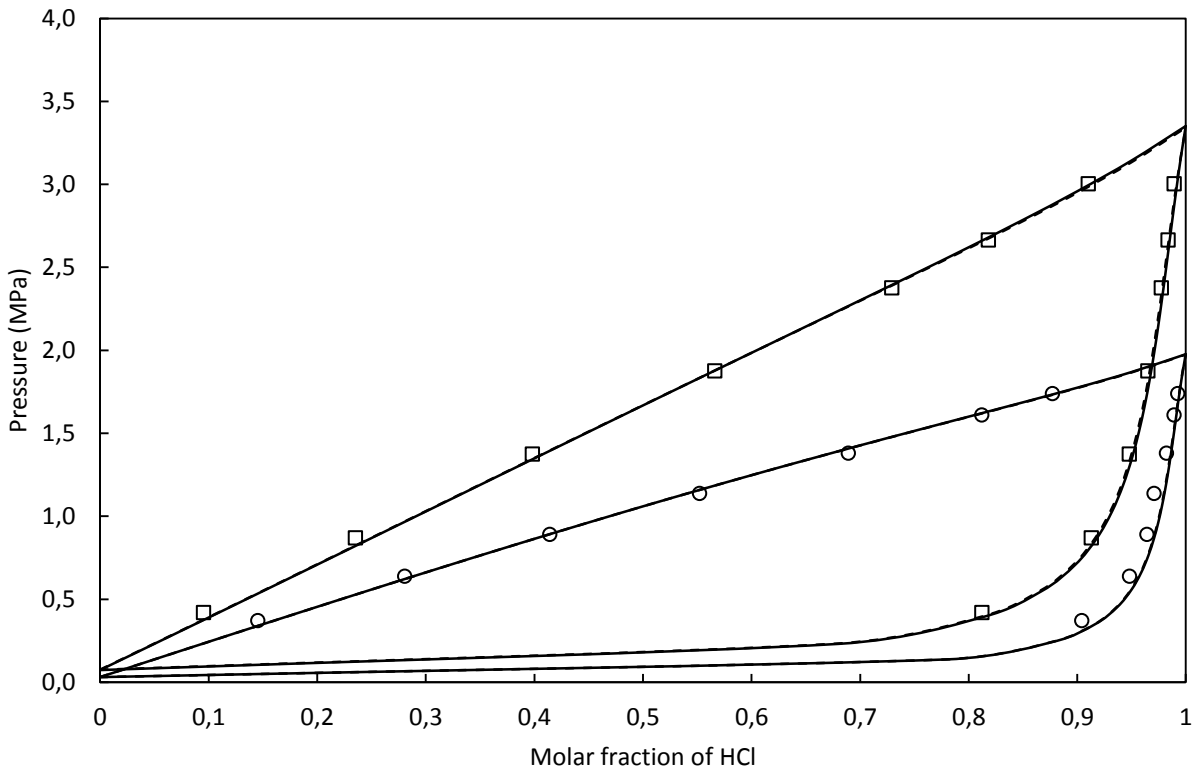


Figure 3 : P - x - y phase diagram of $\text{HCl} - \text{R1233zd}(E)$ binary system. Experimental values: 263.21 K (\circ) and 283.28 K (\square). Modelling results: Peng-Robinson (Solid lines), NEoS (Dashed lines).

Table 4 : Experimental and modeling vapor-liquid equilibria of $\text{HCl}(1) + \text{R1233zd}(E)(2)$ at temperature T , liquid composition x , gas composition y , and pressure P for a number of samples n , and associated standard deviation of composition σ

Experimental				NEoS				Peng-Robinson			
P	n	x_1	σ_{x1}	n	y_1	σ_{y1}	P_{calc}	$y_{1,\text{calc}}$	P_{calc}	$y_{1,\text{calc}}$	
MPa							MPa		MPa		
$T = 263.21 \text{ K}$											
0.3724	7	0.145	0.0005	5	0.904	0.0040	0.3385	0.9131	0.3238	0.9101	
0.6398	7	0.280	0.0003	7	0.948	0.002	0.6209	0.9553	0.5975	0.9546	
0.8918	8	0.414	0.001	6	0.964	0.0006	0.8916	0.9714	0.8659	0.9715	
1.1387	8	0.552	0.002	6	0.971	0.0004	1.1584	0.9805	1.1388	0.9811	
1.3812	7	0.689	0.002	8	0.982	0.001	1.4076	0.9867	1.4036	0.9876	
1.6113	15	0.812	0.0009	6	0.989	0.0003	1.6198	0.9913	1.6377	0.9922	

1.7402	7	0.877	0.001	6	0.992	0.0002	1.7322	0.9938	1.7636	0.9946
T = 283.28 K										
0.4208	10	0.0951	0.0006	5	0.812	0.001	0.3751	0.8019	0.3732	0.8026
0.8710	7	0.235	0.0006	6	0.913	0.0003	0.8217	0.9116	0.8179	0.9128
1.3758	7	0.398	0.001	5	0.948	0.0003	1.3438	0.9487	1.3397	0.9501
1.8770	7	0.566	0.001	7	0.965	0.0002	1.8772	0.9669	1.8768	0.9683
2.3774	10	0.729	0.003	8	0.977	0.0002	2.3892	0.9787	2.3976	0.9800
2.6658	7	0.818	0.003	12	0.984	0.0002	2.6730	0.9846	2.6883	0.9857
3.0044	14	0.910	0.001	6	0.989	0.0002	2.9844	0.9912	3.0077	0.9920

$U(T, k=2) = 0.1 \text{ K}$, $U(P, k=2) = 0.003 \text{ MPa}$, $U(x_1, y_1, k=2) = 0.04$.

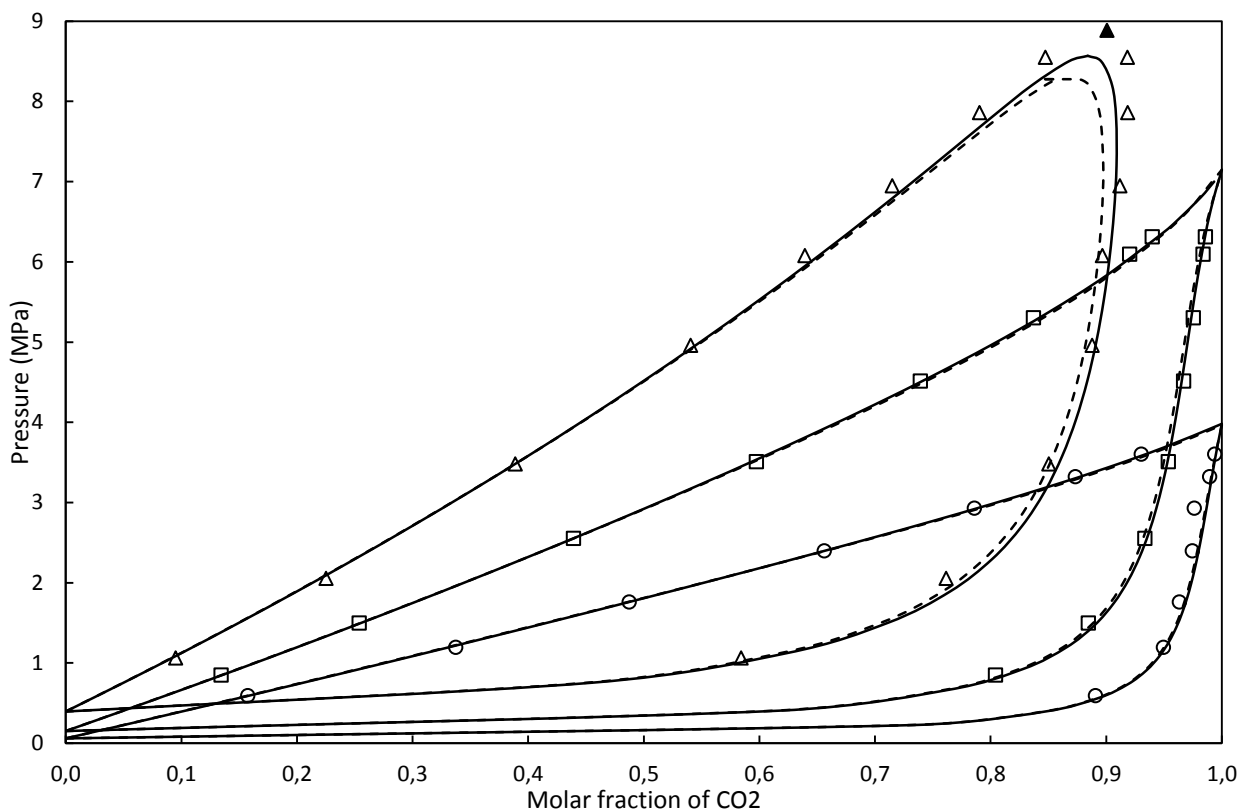


Figure 4 : P-xy phase diagram of $\text{CO}_2 - \text{R1233zd}(E)$ binary system. Experimental values: 278.28 K (\circ), 302.59 K (\square) and 333.17 K (Δ). Modelling results: Peng-Robinson (Solid lines), NEoS (Dashed lines), \blacktriangle : Predicted critical point at 333.17 K

Table 5 : Experimental and modeling vapor-liquid equilibria of $CO_2(1) + R1233zd(E)(2)$ at temperature T, liquid composition x, gas composition y, and pressure P for a number of samples n, and associated standard deviation of composition σ

Experimental				NEoS			Peng-Robinson			
P	n	x ₁	σ_{x1}	n	y ₁	σ_{y1}	P _{calc}	y _{1,calc}	P _{calc}	y _{1,calc}
MPa							MPa		MPa	
T = 278.28 K										
0.5924	8	0.157	0.003	7	0.891	0.0006	0.5929	0.8972	0.5888	0.8979
1.1946	8	0.337	0.004	7	0.949	0.0003	1.2214	0.9511	1.2170	0.9523
1.7595	7	0.487	0.008	6	0.963	0.0008	1.7595	0.9676	1.7603	0.9689
2.3972	14	0.656	0.006	6	0.974	0.0008	2.3825	0.9787	2.3972	0.9799
2.9288	8	0.786	0.007	7	0.976	0.0006	2.8877	0.9855	2.9186	0.9866
3.3214	8	0.873	0.007	6	0.989	0.0009	3.2602	0.9903	3.3033	0.9912
3.6022	7	0.930	0.003	5	0.994	0.0004	3.5325	0.9940	3.5828	0.9946
T = 302.59 K										
0.8490	5	0.134	0.0002	5	0.804	0.0003	0.8490	0.8099	0.8483	0.8128
1.4973	5	0.254	0.001	6	0.884	0.0006	1.4969	0.8884	1.4973	0.8915
2.5524	5	0.439	0.0005	6	0.933	0.0005	2.5578	0.9319	2.5641	0.9352
3.5084	5	0.597	0.0008	5	0.954	0.0003	3.5274	0.9500	3.5443	0.9533
4.5134	11	0.739	0.0008	5	0.967	0.0003	4.4778	0.9619	4.5075	0.9650
5.3020	9	0.837	0.0003	5	0.975	0.0002	5.2266	0.9702	5.2624	0.9729
6.0944	6	0.920	0.0004	6	0.984	0.0003	6.0014	0.9797	6.0333	0.9816
6.3110	5	0.940	0.0004	5	0.986	0.0003	6.2188	0.9828	6.2475	0.9844
T = 333.17 K										
1.0618	8	0.0949	0.002	8	0.584	0.004	1.0887	0.6112	1.0956	0.6188
2.0540	6	0.225	0.0008	4	0.761	0.006	2.1078	0.7813	2.1218	0.7890

3.4804	10	0.389	0.0003	6	0.850	0.002	3.5113	0.8528	3.5245	0.8607
4.9583	8	0.540	0.0009	12	0.888	0.0009	4.9583	0.8821	4.9583	0.8907
6.0773	6	0.639	0.003	6	0.897	0.0005	5.9938	0.8924	5.9774	0.9020
6.9470	6	0.715	0.001	6	0.912	0.002	6.8377	0.8963	6.8067	0.9071
7.8593	12	0.790	0.002	8	0.918	0.002	7.7054	0.8946	7.6698	0.9081
8.5487	6	0.847	0.0004	7	0.918	0.001	8.5487	0.8473	8.5487	0.8473

$U(T, k=2) = 0.08 \text{ K}$, $U(P, k=2) = 0.01 \text{ MPa}$, $U(x_1, y_1, k=2) = 0.04$.

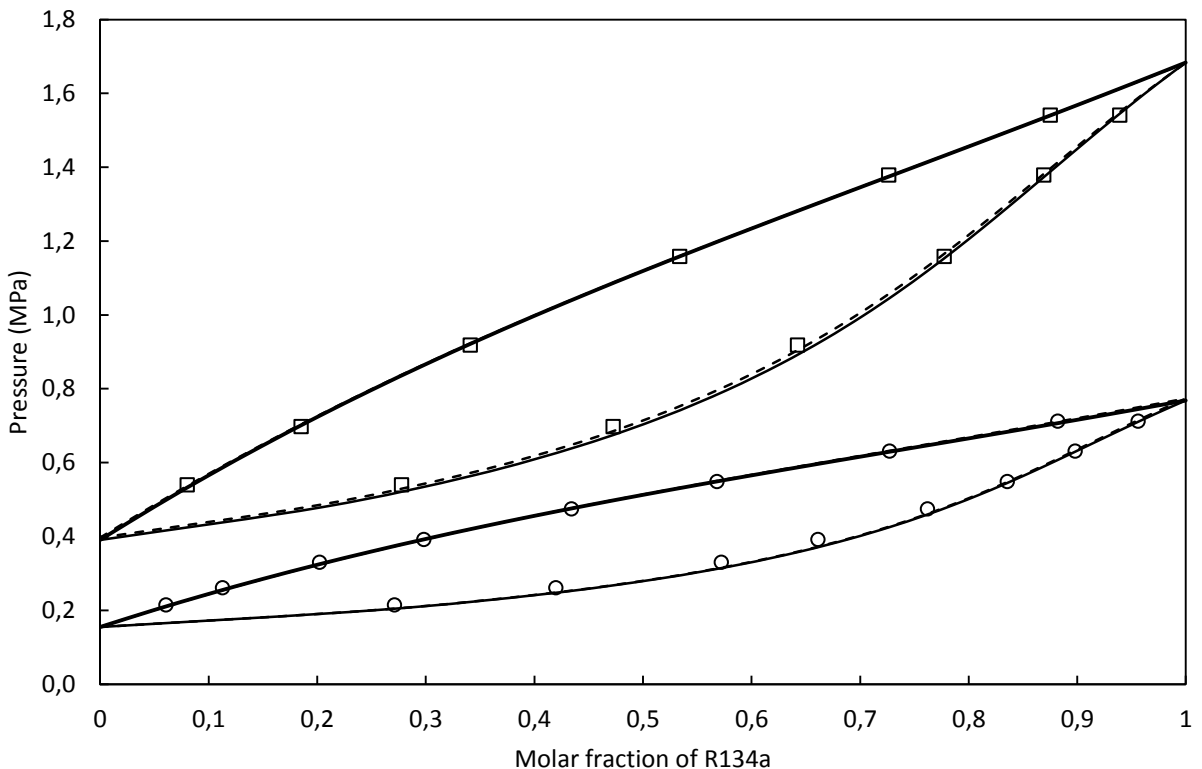


Figure 5 : P-xy phase diagram of R134a–R1233zd(E) binary system. Experimental values: 303.07 K (○) and 333.23 K (□). Modelling results: Peng-Robinson (Solid lines), NEoS (Dashed lines).

Table 6 : Experimental and modeling vapor-liquid equilibria of R134a(1) + R1233zd(E)(2) at temperature T , liquid composition x , gas composition y , and pressure P for a number of samples n , and associated standard deviation of composition σ

Experimental					NEoS			Peng-Robinson		
P	n	x ₁	σ_{x1}	n	y ₁	σ_{y1}	P _{calc}	y _{1,calc}	P _{calc}	y _{1,calc}

MPa				MPa				MPa			
T = 303.07 K											
0.2147	15	0.0605	0.0002	5	0.271	0.001	0.2139	0.3025	0.2102	0.2944	
0.2612	6	0.113	0.0005	5	0.420	0.0004	0.2604	0.4476	0.2548	0.4398	
0.3302	5	0.202	0.0008	5	0.572	0.001	0.3322	0.5955	0.3248	0.5908	
0.3919	7	0.298	0.002	11	0.661	0.0006	0.3997	0.6898	0.3920	0.6886	
0.4747	9	0.434	0.002	6	0.762	0.0008	0.4816	0.7748	0.4758	0.7774	
0.5488	8	0.568	0.001	7	0.835	0.0002	0.5513	0.8338	0.5491	0.8387	
0.6312	10	0.727	0.001	7	0.898	0.0003	0.6262	0.8921	0.6295	0.8980	
0.7123	5	0.882	0.0007	5	0.956	0.0002	0.6972	0.9491	0.7069	0.9534	
T = 333.23 K											
0.5399	6	0.0801	0.0004	6	0.278	0.0009	0.5358	0.2951	0.5323	0.2951	
0.6977	7	0.185	0.0007	6	0.472	0.0003	0.7057	0.4961	0.7010	0.4976	
0.9184	7	0.341	0.0007	6	0.642	0.0009	0.9255	0.6566	0.9215	0.6603	
1.1584	6	0.534	0.0006	6	0.777	0.0008	1.1584	0.7747	1.1585	0.7798	
1.3789	6	0.726	0.0006	5	0.869	0.001	1.3680	0.8649	1.3746	0.8697	
1.5411	6	0.875	0.001	7	0.939	0.002	1.5267	0.9340	1.5402	0.9371	

U(T, k=2) = 0.08 K, U(P, k=2) = 0.01 MPa, U(x₁,y₁,k=2) = 0.04.

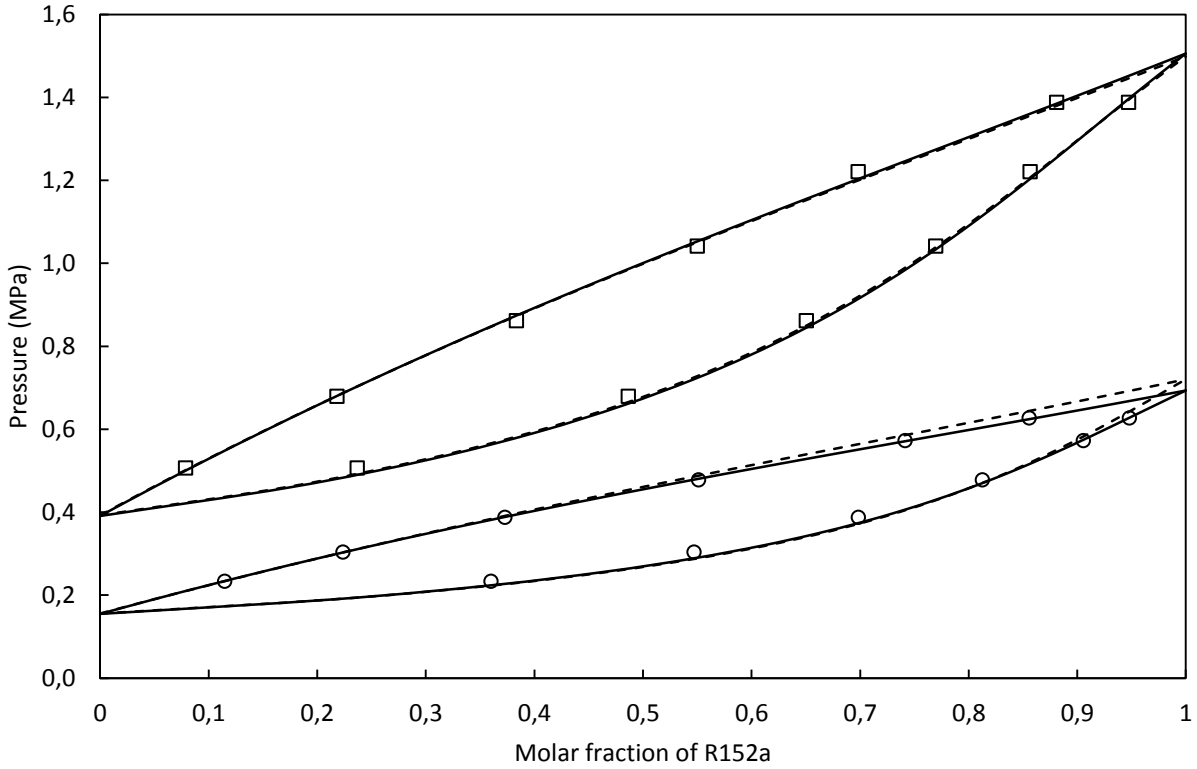


Figure 6 : *P*-*x*-*y* phase diagram of R152a–R1233zd(E) binary system. Experimental values: 303.10 K (○) and 333.23 K (□). Modelling results: Peng-Robinson (Solid lines), NEoS (Dashed lines).

Table 7 : Experimental and modeling vapor-liquid equilibria of R152a(1) + R1233zd(E)(2) at temperature *T*, liquid composition *x*, gas composition *y*, and pressure *P* for a number of samples *n*, and associated standard deviation of composition *σ*

Experimental				NEoS				Peng-Robinson			
P MPa	n	x ₁	σ _{x1}	n	y ₁	σ _{y1}	P _{calc} MPa	y _{1,calc}	P _{calc} MPa	y _{1,calc}	
T = 303.10 K											
0.2338	8	0.114	0.00047	5	0.360	0.00075	0.2313	0.3873	0.2336	0.3953	
0.3042	5	0.224	0.00107	9	0.547	0.00086	0.2998	0.5720	0.3024	0.5766	
0.3880	7	0.373	0.00214	10	0.698	0.00134	0.3880	0.7191	0.3880	0.7186	
0.4783	9	0.551	0.00203	9	0.812	0.00061	0.4871	0.8274	0.4801	0.8229	
0.5729	8	0.741	0.00442	9	0.905	0.00011	0.5885	0.9085	0.5707	0.9028	
0.6275	7	0.856	0.00093	9	0.948	0.00031	0.6495	0.9499	0.6240	0.9454	

T = 333.23 K

0.5069	6	0.0786	0.00019	6	0.237	0.00057	0.5005	0.2528	0.4997	0.2553
0.6797	5	0.218	0.00163	6	0.486	0.00034	0.6796	0.5023	0.6797	0.5062
0.8620	9	0.383	0.00068	5	0.650	0.00053	0.8724	0.6671	0.8736	0.6713
1.0418	7	0.550	0.00148	5	0.770	0.00051	1.0498	0.7763	1.0524	0.7801
1.2212	6	0.698	0.00212	5	0.856	0.00121	1.1986	0.8532	1.2026	0.8564
1.3883	12	0.880	0.00036	7	0.947	0.00082	1.3783	0.9402	1.3845	0.9419

$U(T, k=2) = 0.08 \text{ K}$, $U(P, k=2) = 0.001 \text{ MPa}$, $U(x_1, y_1, k=2) = 0.04$.

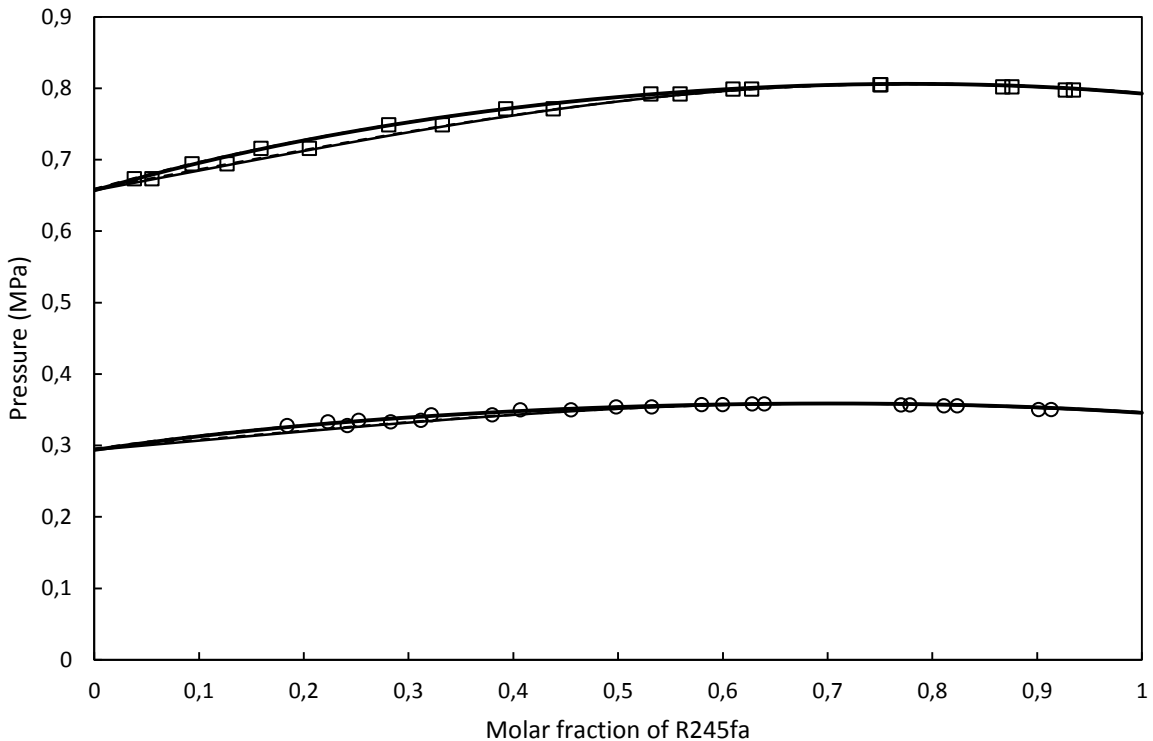


Figure 7 : P-xy phase diagram of R245fa–R1233zd(E) binary system. Experimental values: 323.27 K (○) and 353.27 K (□). Modelling results: Peng-Robinson (Solid lines), NEoS (Dashed lines).

Table 8 : Experimental and modeling vapor-liquid equilibria of R245fa(1) + R1233zd(E)(2) at temperature T, liquid composition x, gas composition y, and pressure P for a number of samples n, and associated standard deviation of composition σ

	Experimental	NEoS	Peng-Robinson
--	--------------	------	---------------

P	n	x₁	σ_{x1}	n	y₁	σ_{y1}	P_{calc}	y_{1,calc}	P_{calc}	y_{1,calc}	
						MPa		MPa		MPa	
T = 323.27 K											
0.3277	6	0.184	0.0002	8	0.241	0.0004	0.3261	0.2455	0.3257	0.2473	
0.3329	6	0.223	0.0002	6	0.283	0.0001	0.3311	0.2872	0.3308	0.2890	
0.3350	6	0.252	0.0003	6	0.312	0.0008	0.3345	0.3170	0.3342	0.3188	
0.3427	6	0.322	0.0001	10	0.380	0.0002	0.3415	0.3833	0.3414	0.3850	
0.3497	6	0.406	0.0001	12	0.455	0.0003	0.3484	0.4584	0.3483	0.4597	
0.3538	8	0.498	0.0001	7	0.532	0.0003	0.3538	0.5348	0.3538	0.5356	
0.3570	9	0.580	0.0002	6	0.600	0.0003	0.3570	0.6013	0.3570	0.6016	
0.3580	13	0.628	0.0002	11	0.639	0.0002	0.3581	0.6407	0.3581	0.6407	
0.3501	9	0.913	0.0002	6	0.901	0.0004	0.3530	0.9005	0.3527	0.8999	
0.3553	6	0.824	0.0003	5	0.811	0.0002	0.3571	0.8108	0.3569	0.8101	
0.3566	6	0.778	0.0002	5	0.770	0.0002	0.3582	0.7693	0.3581	0.7686	
T = 353.27 K											
0.6732	8	0.0381	0.0002	7	0.0549	0.0001	0.6739	0.0555	0.6727	0.0561	
0.6941	12	0.0932	0.0003	6	0.127	0.0007	0.6941	0.1290	0.6932	0.1301	
0.7157	7	0.159	0.0006	7	0.205	0.0007	0.7155	0.2082	0.7149	0.2097	
0.7487	8	0.281	0.0009	6	0.332	0.0009	0.7481	0.3375	0.7480	0.3390	
0.7711	6	0.393	0.0008	6	0.438	0.0007	0.7711	0.4428	0.7712	0.4441	
0.7919	6	0.531	0.0005	5	0.559	0.0009	0.7914	0.5642	0.7915	0.5648	
0.7987	6	0.610	0.0002	9	0.627	0.0009	0.7991	0.6312	0.7992	0.6315	
0.8048	5	0.751	0.0001	6	0.750	0.0006	0.8059	0.7538	0.8060	0.7536	
0.8018	5	0.876	0.0003	5	0.867	0.0005	0.8039	0.8701	0.8037	0.8697	
0.7974	7	0.934	0.0001	6	0.927	0.0007	0.8001	0.9292	0.7997	0.9289	

$$U(T, k=2) = 0.1 \text{ K}, U(P, k=2) = 0.01 \text{ MPa}, U(x_1, y_1, k=2) = 0.04.$$

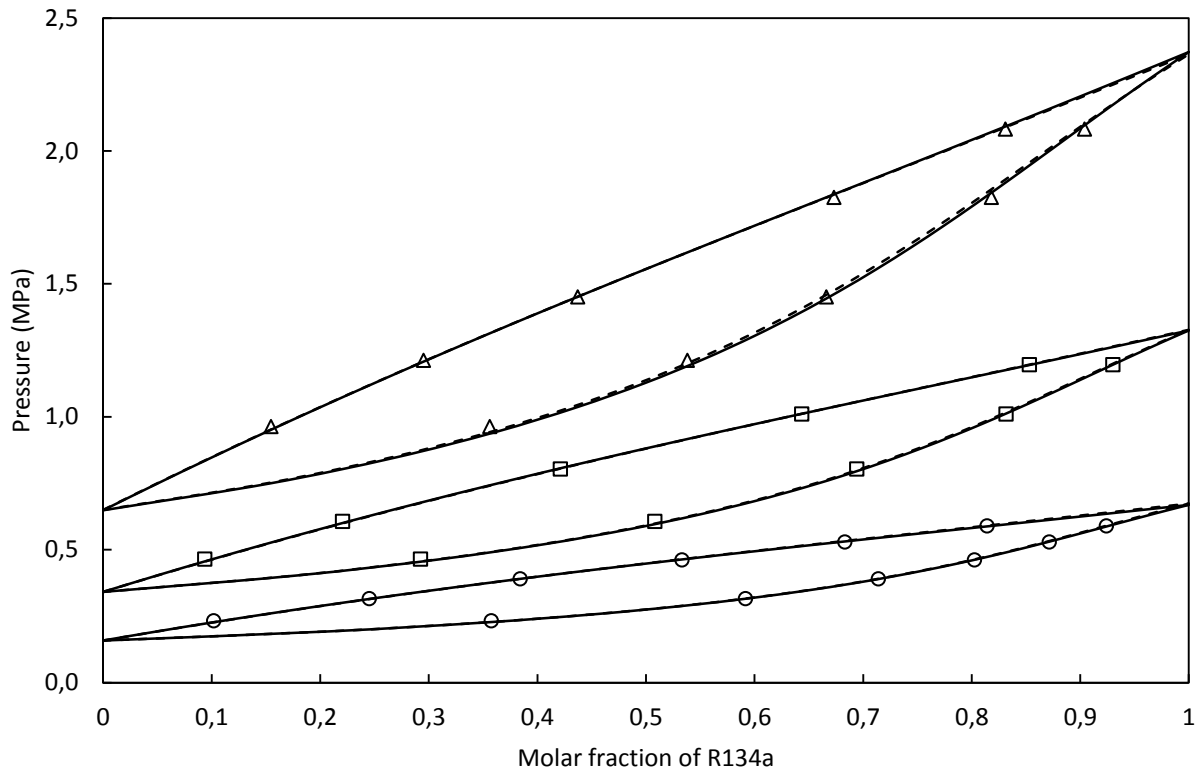


Figure 8 : P-xy phase diagram of R134a – R1233xf binary system. Experimental values: 298.30 K (○), 323.38 K (□) and 348.27 K (Δ). Modelling results: Peng-Robinson (Solid lines), NEoS (Dashed lines).

Table 9 : Experimental and modeling vapor-liquid equilibria of R134a(1) + R1233xf(2) at temperature T, liquid composition x, gas composition y, and pressure P for a number of samples n, and associated standard deviation of composition σ

Experimental				NEoS				Peng-Robinson			
P MPa	n	x ₁	σ _{x1}	n	y ₁	σ _{y1}	P _{calc} MPa	y _{1,calc}	P _{calc} MPa	y _{1,calc}	
T = 298.30 K											
0.2327	7	0.102	0.0009	6	0.357	0.0008	0.2271	0.3527	0.2275	0.3548	
0.3161	6	0.245	0.001	6	0.592	0.0009	0.3145	0.5879	0.3150	0.5899	
0.3905	6	0.384	0.001	6	0.714	0.0006	0.3905	0.7136	0.3906	0.7150	
0.4617	8	0.533	0.001	7	0.802	0.0003	0.4643	0.8032	0.4635	0.8039	
0.5291	11	0.683	0.001	9	0.871	0.0004	0.5330	0.8718	0.5311	0.8721	

0.5896	6	0.814	0.002	6	0.924	0.0005	0.5907	0.9244	0.5877	0.9244
--------	---	-------	-------	---	-------	--------	--------	--------	--------	--------

T = 323.38 K

0.4647	10	0.0935	0.0007	9	0.292	0.001	0.4546	0.2912	0.4551	0.2942
0.6065	7	0.220	0.0006	6	0.508	0.001	0.5984	0.5090	0.5995	0.5129
0.8036	6	0.421	0.001	6	0.694	0.002	0.8044	0.6986	0.8055	0.7021
1.0105	7	0.643	0.0009	10	0.832	0.0006	1.0104	0.8287	1.0105	0.8311
1.1960	6	0.853	0.0002	7	0.930	0.0005	1.1954	0.9283	1.1941	0.9294

T = 348.27 K

0.9633	6	0.154	0.0008	7	0.356	0.001	0.9515	0.3642	0.9508	0.3686
1.2124	6	0.295	0.002	6	0.538	0.002	1.2074	0.5419	1.2070	0.5477
1.4510	6	0.437	0.002	14	0.666	0.001	1.4509	0.6630	1.4510	0.6690
1.8252	6	0.673	0.001	6	0.818	0.001	1.8348	0.8112	1.8362	0.8160
2.0822	7	0.831	0.0008	4	0.904	0.0005	2.0880	0.8993	2.0914	0.9024

U(T, k=2) = 0.1 K, U(P, k=2) = 0.01 MPa, U(x₁,y₁,k=2) = 0.02.

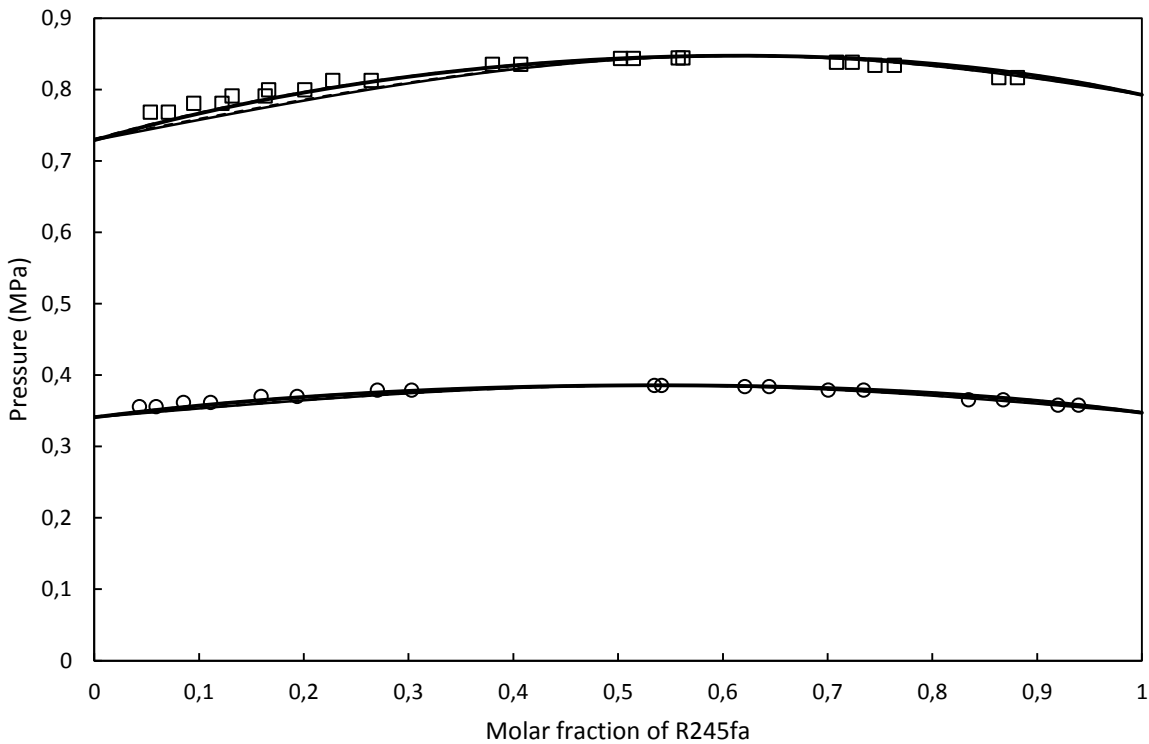


Figure 9 : P-xy phase diagram of R245fa – R1233xf binary system. Experimental values: 323.40 K (○) and 353.27 K (□). Modelling results: Peng-Robinson (Solid lines), NEoS (Dashed lines).

Table 10 : Experimental and modeling vapor-liquid equilibria of R152a(1) + R1233xf(2) at temperature T, liquid composition x, gas composition y, and pressure P for a number of samples n, and associated standard deviation of composition σ

Experimental						NEoS		Peng-Robinson		
P	n	x ₁	σ_{x1}	n	y ₁	σ_{y1}	P _{calc}	y _{1,calc}	P _{calc}	y _{1,calc}
MPa						MPa		MPa		
T = 323.40 K										
0.3560	7	0.0430	0.0001	7	0.0589	0.0002	0.3487	0.0606	0.3485	0.0609
0.3619	8	0.0850	0.0001	8	0.111	0.0003	0.3553	0.1147	0.3551	0.1152
0.3703	9	0.159	0.0002	6	0.194	0.0003	0.3650	0.2005	0.3649	0.2012
0.3791	12	0.270	0.0002	7	0.303	0.0003	0.3757	0.3118	0.3757	0.3125
0.3857	7	0.541	0.0002	8	0.534	0.0002	0.3858	0.5404	0.3858	0.5402
0.3841	6	0.644	0.001	10	0.621	0.0004	0.3841	0.6237	0.3841	0.6231

0.3581	5	0.939	0.0003	10	0.920	0.0004	0.3586	0.9159	0.3582	0.9153
0.3792	6	0.734	0.0004	6	0.700	0.0002	0.3800	0.7009	0.3799	0.7001
0.3656	8	0.867	0.0002	6	0.834	0.0003	0.3683	0.8313	0.3681	0.8304
T = 353.27 K										
0.7685	8	0.0534	0.0003	14	0.0706	0.0002	0.7511	0.0731	0.7499	0.0737
0.7809	12	0.0948	0.0002	6	0.122	0.0005	0.7656	0.1251	0.7645	0.1261
0.7912	11	0.131	0.0001	12	0.163	0.0003	0.7772	0.1683	0.7763	0.1695
0.7998	6	0.166	0.0001	6	0.201	0.0003	0.7874	0.2074	0.7866	0.2087
0.8129	6	0.228	0.0003	6	0.264	0.0002	0.8031	0.2717	0.8025	0.2731
0.8355	7	0.380	0.0002	14	0.407	0.0003	0.8313	0.4150	0.8311	0.4162
0.8437	7	0.502	0.0002	7	0.514	0.0003	0.8437	0.5201	0.8437	0.5208
0.8169	11	0.881	0.0003	6	0.863	0.0003	0.8234	0.8601	0.8233	0.8595
0.8341	7	0.764	0.0003	9	0.745	0.0005	0.8403	0.7448	0.8403	0.7443
0.8384	6	0.723	0.0002	9	0.708	0.0006	0.8437	0.7084	0.8437	0.7080
0.8445	6	0.557	0.0006	8	0.562	0.0008	0.8465	0.5662	0.8465	0.5667

U(T, k=2) = 0.1 K, U(P, k=2) = 0.0008 MPa, U(x₁,y₁,k=2) = 0.02.

4. Modelling

In order to correlate the data, bubble pressure algorithm³⁷ (and isothermal flash algorithm³⁸ in the case of CO₂-R1233zd(E) at 333K) have been used with the Peng-Robinson equation of state²⁶ (PR EoS) and a modified Patel-Teja equation of state, referred as NEoS²⁷.

$$P = \frac{RT}{v-b} - \frac{a(T)}{v(v+b)+b(v-b)} \quad (1)$$

$$P = \frac{RT}{v-b} - \frac{a(T)}{v(v+b)+c(v-b)-b^2} \quad (2)$$

$$a(T) = a_c \alpha(T) \quad (3)$$

$$a_c = \Omega_a \frac{R^2 T_c^2}{P_c} \quad (4)$$

$$b = \Omega_b \frac{RT_c}{P_c} \quad (5)$$

$$c = \Omega_c \frac{RT_c}{P_c} \quad (6)$$

In the Peng-Robinson case, $\Omega_a = 0.45724$ and $\Omega_b = 0.0778$, while with the NEoS we have to solve system of equations 7 to 9 :

$$\Omega_a = 1 - 3Z_{c,opt}(1 - Z_{c,opt}) + 3(1 - 2Z_{c,opt})\Omega_b + 2\Omega_b^2 \quad (7)$$

$$\Omega_b^3 + (1 - 3Z_{c,opt})\Omega_b^2 + 3Z_{c,opt}^2\Omega_b - Z_{c,opt}^3 = 0 \quad (8)$$

$$\Omega_c = 1 - 3Z_{c,opt} \quad (9)$$

Where $Z_{c,opt}$ is an optimized critical compressibility factor adjusted from the experimental VLE and liquid density data in order to improve the prediction of liquid densities.

Both models are coupled with the Mathias-Copeman (MC) alpha function²⁸ :

If $T < T_c$:

$$\alpha(T) = \left[1 + m_1 \left(1 - \sqrt{\frac{T}{T_c}} \right) + m_2 \left(1 - \sqrt{\frac{T}{T_c}} \right)^2 + m_3 \left(1 - \sqrt{\frac{T}{T_c}} \right)^3 \right]^2 \quad (10)$$

If $T \geq T_c$:

$$\alpha(T) = \left[1 + m_1 \left(1 - \sqrt{\frac{T}{T_c}} \right) \right]^2 \quad (11)$$

m_1 , m_2 and m_3 are three adjustable parameters fitted on the experimental pure component data. For the mixtures, the classical van der Waals (vdW) mixing and combining rules were used for the calculations, as defined by:

$$a = \sum_{i=1}^N \sum_{j=1}^N z_i z_j a_{ij} \quad (12)$$

$$b = \sum_{i=1}^N z_i b_i \quad (13)$$

$$c = \sum_{i=1}^N z_i c_i \quad (14)$$

$$a_{ij} = (1 - k_{ij}) \sqrt{a_i a_j} \quad (15)$$

Where z_i is the mole fraction of the component i, a_i the energy parameter, b_i is the covolume parameter of the component i and k_{ij} is the binary interaction parameter. N is the number of components in the system. The vdW mixing rules were chosen for their simplicity, ease of computing and also to be able to use a predictive binary interaction parameter. The binary interaction parameter was fitted on experimental VLE data to account for the molecular

interactions occurring, and the α -function parameters (m_1 , m_2 , m_3) were fitted to the pure compound data, in order to accurately represent the vapor pressures. The objective function used to fit the model to the experimental data, for the PR – MC combination for pure components is given by:

$$F_{objP} = \frac{100}{N} \left[\sum_1^N \left(\frac{P_{exp} - P_{cal}}{P_{exp}} \right)^2 \right] \quad (16)$$

We add the liquid molar volume to this objective function in the case of the NEoS – MC combination:

$$F_{objPv} = \frac{100}{N} \left[\sum_1^N \left(\frac{P_{exp} - P_{cal}}{P_{exp}} \right)^2 + \sum_1^N \left(\frac{v_{L,exp} - v_{L,cal}}{v_{L,exp}} \right)^2 \right] \quad (17)$$

In the case of mixtures, the objective function used is of the form:

$$F_{objPy} = \frac{100}{N} \left[\sum_1^N \left(\frac{P_{exp} - P_{cal}}{P_{exp}} \right)^2 + \sum_1^N \left(\frac{y_{1,exp} - y_{1,cal}}{y_{1,exp}} \right)^2 \right] \quad (18)$$

Where N is the number of points, P_{exp} the experimental bubble pressure, P_{calc} the calculated bubble pressure, $v_{L,exp}$ the experimental liquid molar volume, $v_{L,calc}$ the calculated liquid molar volume, $y_{1,exp}$ the experimental vapor molar fraction of component 1 and $y_{1,calc}$ the calculated vapor molar fraction of component 1.

The critical temperature, pressure and the acentric factor of the refrigerants, used for the modeling, are reported in Table 11.

Table 11 : Pure components molecular properties, from REFPROP 10.0 (values for the R1233xf are taken elsewhere) with critical temperature Tc, critical pressure Pc, acentric factor ω , and molecular weight MM

Compounds	Tc	Pc	ω	MM
	K	MPa		g.mol ⁻¹
Butane	425.13	3.796	0.201	58.122
HCl	324.68	8.314	0.129	36.461
CO₂	304.13	7.377	0.224	44.010
R134a	374.21	4.059	0.327	102.03
R152a	386.41	4.517	0.275	66.05
R245fa	427.01	3.651	0.378	134.05
R1233zd(E)	439.6	3.624	0.303	130.50
R1233xf²⁴	439.98	3.322	0.187	130.50

We have used vapor pressure data found in the literature when possible or the vapor pressure predicted by REFPROP 10.0 otherwise. Values of the Mathias – Copeman α -function parameters and optimized Z_c are given in Table 12. Parameters of the Antoine equation (equation 19) are computed and given in Table 12, as the equation is useful for initialization in the bubble point algorithm.

$$\log_{10}(P^{sat}) = A - \frac{B}{T+C} \quad (19)$$

With P^{sat} , the vapor pressure of pure component in bar, T , the temperature in K and A, B, C, three adjustable parameters referred as m_1 , m_2 and m_3 , respectively, in Table 12. Standard deviation of these parameters are provided in supporting informations.

Indicators AAD and BIAS for a thermodynamic quantity (U) are defined by Equations 20 and 21:

$$AAD_U = \frac{100}{N} \left(\frac{|U_{exp} - U|}{U_{exp}} \right) \quad (20)$$

$$BIAS_U = \frac{100}{N} \left(\frac{U_{exp} - U_{cal}}{U_{exp}} \right) \quad (21)$$

Table 12 : Optimized parameters m_1 , m_2 and m_3 of the Mathias-Copeman α -function for use with NEoS and Peng-Robinson equations of state, and parameters of the Antoine equation, with absolute average deviation AAD, and BIAS for vapor pressure and liquid molar volume of pure components, along with experimental critical compressibility factor Z_c

Component	Z_c^*	Model	m_1	m_2	m_3	Pressure		Molar volume	
						AAD	BIAS	AAD	BIAS
						%	%	%	%
Butane ³⁹	0.2829	Antoine	4.8494	1581.1	58.0851	0.3	-0.06	/	/
		NEoS	0.4099	0.2118	-0.6214	0.3	-0.2	4.6	-0.3
	0.2772	PR	0.757	-1.7872	9.2248	0.2	-0.006	7.5	-6.4
		Antoine	4.8439	1026.5	25.9588	5.7	-5.4	/	/
HCl ⁴⁰	0.2772	NEoS	0.3108	0.1611	0.1331	0.2	-0.008	1.9	-0.02
		PR	0.6127	-0.3747	0.6941	0.2	-0.05	4.2	-4.2
CO ₂ ⁴¹	0.2889	Antoine	4.8089	921.6	8.9734	0.3	-0.1	/	/
		NEoS	0.4584	0.1425	0.6610	0.3	0.1	2.0	-0.04

		PR	0.7242	-0.5660	2.8556	0.07	-0.02	4.2	-1.3
		Antoine	4.9690	1349.5	27.2708	0.7	-0.4	/	/
R134a ⁴²	0.2744	NEoS	0.5408	-0.4741	4.5186	0.3	-0.1	4.5	-0.4
		PR	0.8946	-0.7698	3.0513	0.1	-0.004	9.1	-9.1
		Antoine	4.6955	1197.6	7.0990	0.3	0.1	/	/
R152a ⁴³	0.2642	NEoS	0.4622	-0.3204	-1.0231	0.7	0.4	3.6	-0.09
		PR	0.8507	-1.2689	5.149	0.1	0.1	17.6	17.6
		Antoine	4.4789	1176.8	-24.602	0.2	-0.05	/	/
R245fa ⁴⁴	0.2862	NEoS	0.6518	-0.4073	4.2580	0.2	0.08	0.7	-0.0002
		PR	0.9490	-0.7357	3.6061	0.05	-0.003	2.6	-1.1
		Antoine	4.5783	1329.9	0.2769	1.4	-1.0	/	/
R1233zd(E) ⁴⁵	0.2821	NEoS	0.5273	0.2070	0.5399	0.9	0.5	2.5	0.01
		PR	0.8532	-0.4738	1.4187	0.9	0.6	2.9	-0.3
		Antoine	4.5642	1332,4	7.0694	0.001	-0.0007	/	/
R1233xf ²⁴	0.2666	NEoS	0.0390	3.1507	-6.7603	0.09	-0.02	1.2	-0.4
		PR	0.3764	2.7635	-6.6534	0.06	0.0005	7.7	-7.7

For the mixtures, binary interaction parameters for both models as well as AAD and BIAS on bubble pressure and vapor molar fraction are provided in Table 13.

Table 13 : Binary interaction parameters k_{ij} , of NEoS and Peng-Robinson equations of state at temperature T , with associated absolute average deviation AAD and BIAS on equilibrium pressure P and gas composition y

System	Model	Temperature	k_{ij}	AAD P	BIAS P	AAD y_1	BIAS y_1
		K		%	%	%	%
Butane +	NEoS	323.27	0.0430	0.6	-0.3	0.6	0.6

R1233zd(E)		353.23	0.0418				
Peng- Robinson	323.27	0.0553		0.5	-0.2	0.7	-0.6
	353.23	0.0465					
HCl + R1233zd(E)	263.21	0.0296		2.8	2.1	0.5	-0.3
	283.28	0.0299					
Peng- Robinson	263.21	0.0380		2.9	2.0	0.6	-0.4
	283.28	0.0378					
CO ₂ + R1233zd(E)	278.28	0.0168					
	NEoS	302.59	0.0193	1.3	0.01	1.0	0.2
R134a + R1233zd(E)	333.17	0.0079					
	278.28	0.0259					
Peng- Robinson	302.59	0.0288	1.1	-0.04	0.9	-0.4	
	333.17	0.0157					
R152a + R1233zd(E)	303.07	0.0473		0.7	0.4	2.4	-2.2
	333.23	0.0536					
Peng- Robinson	303.07	0.0512		0.8	0.6	3.0	-2.9
	333.23	0.0574					
R245fa + R1233zd(E)	303.10	0.0286		1.4	-0.1	3.4	-3.2
	333.23	0.0410					
Peng- Robinson	303.10	0.0360		0.7	0.2	3.4	-3.2
	333.23	0.0428					
R134a +	NEoS	323.27	0.0347		0.2	-0.03	0.9
		353.27	0.0329				-0.9
Peng- Robinson	323.27	0.0388		0.3	0.01	1.2	-1.2
		353.27	0.0373				

R1233xf		323.38	0.0355				
		348.27	0.0402				
		298.30	0.0398				
Peng-Robinson		323.38	0.0434	0.7	0.4	0.8	-0.5
		348.27	0.0477				
		323.40	0.0353				
	NEoS	353.27	0.0367	1.0	0.6	1.9	-1.7
R245fa + R1233xf	Peng-Robinson	323.40	0.0429				
		353.27	0.0454	1.0	0.7	2.2	-2.0

5. Discussions

Pure components. The NEoS used in this paper has similar performances, or slightly less performant, than PR EoS for representing vapor pressure of pure components, but it is much more appropriate for liquid densities (especially because parameters are regressed from liquid densities as well).

Butane + R1233zd(E). The $P-x,y$ phase diagram (Figure 2), show that both models depict the experimental data with accuracy, with no appreciable differences. However, the relative volatility plots (Figure S1) show that the Peng-Robinson model seems to be more effective, specifically for representing data points closer to the azeotrope.

From the $P-x,y$ phase diagram we could say that both models depict the experimental data with accuracy with no appreciable differences. However, looking at the relative volatility plots, we can see that, for the 333K data, the PR model seems to be more effective, specifically for representing data points closer to the azeotrope. At the higher temperature of 353K, both models give the same results. Error in butane K-values are plotted in Figure S2. They are all within 3%.

HCl + R1233zd(E). The $P-xy$ phase diagram exhibits typical behavior for a mixture of different size molecules (that we also find in $\text{CO}_2 + \text{R1233zd(E)}$) with negative deviation from Raoult's law.

The error in HCl K-values (Figure S4) is within 1.5% and both models show the same performances. But looking at the relative volatility (Figure S3), we can see large differences between the model and the experimental data at 263.21 K.

CO₂ + R1233zd(E). Like the HCl + R1233zd(E) mixture, we can see a typical $P-xy$ phase diagram for mixtures of different sized molecules. We can also observe the negative deviation from the ideal behavior.

K-values (Figure S6) would be within 5% deviation if not for one result of the NEoS model. Since for the temperature above the critical temperature of CO₂ both models exhibit the same trend in K-value errors, we accept this data point and conclude that NEoS model is less performant than the PR EoS in this case.

Looking at the relative volatility plots (Figure S5), the PR model seems to be doing better at higher temperatures.

R134a + R1233zd(E). *P*-xy phase diagram of R134a + R1233zd(E) are typical of mixture of similar type molecules, with a slight positive deviation from Raoult's law.

K-values (Figure S8) analysis show that models correspond to experimental data within 10%, with the highest deviation at low R134a mole fractions. Deviation in relative volatility (Figure S7) is consistent with this analysis since deviation is a bit higher than 10% (from 7.5 to 13.5% for both models and both temperatures).

R152a + R1233zd(E). The *P*-xy phase diagram is, again, typical of mixture of similar type molecules with a slight positive deviation from ideal behavior. We can notice a difference in vapor pressure prediction between PR and NEoS model (same as with butane).

The error in K-values (Figure S10) are basically within 10% deviation, with the same behavior seen on the R134a + R1233zd(E) mixture, a high deviation at low R152a mole fractions. Relative volatility deviations (Figure S9) are below 20%.

R245fa + R1233zd(E). The *P*-xy phase diagram shows a narrow liquid-vapor equilibria lens with an azeotropic behavior. Both models are undistinguishable. But, enhancing the view of each isotherm, we notice that both models struggle to represent VLE data.

Errors in K-values (Figure S12) are within 3% and, one again, higher deviations are found at the high molar fraction of the more volatile compound. Deviations in relative volatilities (Figure S11) are within 4%.

R134a + R1233xf. Phase diagrams are consistent with a mixture of similar type molecules, with a slight positive deviation from the ideal behavior. Both models exhibit the same performances. Errors in K-values (Figure S14) are all within 4%. Relative volatilities (Figure S13) are within 5.5%.

R245fa + R1233xf. Same interpretations than for the other R245fa mixture. Also, error in K-values (Figure S16) are within 5% with the same trend of high deviation for the low molar fraction of the more volatile component. Relative volatilities (Figure S15) are within 6%, which is consistent with K-values errors.

Overall, binary interaction parameters are similar for PR and NEoS, though they are lesser for the NEoS, meaning that they basically provide the same correction.

6. Conclusions

This paper presents new experimental VLE data for mixtures of refrigerants. Data have been correlated with NEoS and PR EoS with Mathias-Copeman alpha-function and classical mixing rules. Data

representation by these models is not always good (deviation higher than 10%) and one should exercise careful attention when using these data sets.

Mixtures R134a+R1233zd(E), R152a+R1233zd(E) and R134a+R1233xf are similar. They exhibit a near-ideal behavior, showing just a slight positive deviation from Raoult's law.

CO₂ and HCl in mixture with R1233zd(E) are also similar. Their P-xy phase diagrams are typical of type I, according to van Konynenburg and Scott classification⁴⁶, for mixtures of different sized molecules. Though it looks like both NEoS and PR models are struggling to accurately correlate this type of mixtures.

R245fa in mixture with either R1233zd(E) or R1233xf show a similar behavior, with a closed lens and an azeotropic behavior. It looks like it is difficult for both models used in this paper correlate this kind of behavior.

We find a similar kind of phase diagram for the n-Butane+R1233zd(E) mixture, although not as pronounced.

The modified Patel-Teja equation of state has similar performances than the PR EoS for correlating phase equilibria but better represent liquid densities. In order to further the comparison, mixture density measurements are needed.

7. Acknowledgements

This work was possible thank to the ANR (Agence Nationale de Recherche) and the PREDIREF project (Projet-ANR-13-CDII-0008).

Appendices

A. Uncertainty calculations.

Temperature and pressure. Several samplings are made for each composition measurement and the mean is the value presented in the tables of this paper:

$$T = \bar{T} = \frac{1}{n} \sum_{i=1}^n T_i$$

Hence, the uncertainty of the temperature is composed of a type A uncertainty, related to the repeatability of the measurement, and a type B uncertainty, related to the calibration of the temperature probe:

$$u_c(T) = \sqrt{u_{repeatability}^2 + u_{calibration}^2}$$

The repeatability component can be considered equal to the standard deviation s , of the n samplings:

$$u_{repeatability}(T) = s(\bar{T})$$

$$s^2(\bar{T}) = \frac{s^2(T_i)}{n}$$

$$s^2(T_i) = \frac{1}{n-1} \sum_{i=1}^n (T_i - \bar{T})^2$$

Where $s^2(T)$ is the variance and $s(T)$ the standard deviation.

The same can be said for the pressure measurements and the same method of uncertainty assessment is made.

Composition. The uncertainty on the molar liquid and vapor fractions are dependent on the number n of samplings made, of the purity of the components and the uncertainty related to the GC, so that:

$$u_c(z_1) = \sqrt{u_{repeatability}^2 + u_{purity}^2 + u_{calibration}^2}$$

With :

$$u_{repeatability} = \sigma$$

Where σ is the standard deviation (see uncertainty of temperature).

$$u_{purity}^2 = \sqrt{\left(\frac{1-p_1}{\sqrt{3}}\right)^2 + \left(\frac{1-p_2}{\sqrt{3}}\right)^2}$$

With p_1 the purity of the component 1 (the more volatile) and p_2 the purity of the component 2.

Finally, the uncertainty related to the calibration of the GC is a type B uncertainty. Since composition is computed from peak areas:

$$z_1 = \frac{n_1}{n_1 + n_2}$$

Where n_1 and n_2 are mole numbers of component 1 and 2, respectively, calculated from peak areas according to:

$$n_i = A_i S_i^2 + B_i S_i$$

Where A_i and B_i are parameters computed while calibrating the GC and S_i is the peak area of component i . So, the uncertainty is given by:

$$u_{calibration} = \sqrt{\left(\frac{\partial z_1}{\partial n_1}\right)^2 u^2(n_1) + \left(\frac{\partial z_1}{\partial n_2}\right)^2 u^2(n_2)}$$

With:

$$\frac{\partial z_1}{\partial n_1} = \frac{n_2}{(n_1 + n_2)^2}$$

$$\frac{\partial z_1}{\partial n_2} = -\frac{n_1}{(n_1 + n_2)^2}$$

And :

$$u(n_1) = \sqrt{\left(\frac{\partial n_1}{\partial S_1}\right)^2 u^2(S_1) + \left(\frac{\partial n_1}{\partial S_2}\right)^2 u^2(S_2)}$$

With:

$$\frac{\partial n_1}{\partial S_1} = 2A_1 S_1 + B_1$$

$$\frac{\partial n_1}{\partial S_2} = 0$$

Relative uncertainties of the peak areas are given in table 2, so:

$$u_{rel.}(S_1) = \frac{u(S_1)}{S_1} \times 100$$

ASSOCIATED CONTENT

Supporting Information available. Relative volatility plots for all binary systems studied. Error in K-values for all binary systems studied. Values of standard deviation of Antoine's equation parameters with methodology. Methodology for the critical point determination of system CO₂ + R1233zd(E). Values of saturated liquid density of R1233xf, with associated methodology.

- (1) Jouhara, H.; Khordehgah, N.; Almahmoud, S.; Delpech, B.; Chauhan, A.; Tassou, S. A. Waste Heat Recovery Technologies and Applications. *Therm. Sci. Eng. Prog.* **2018**, *6*, 268–289. <https://doi.org/10.1016/j.tsep.2018.04.017>.
- (2) Varga, Z.; Palotai, B. Comparison of Low Temperature Waste Heat Recovery Methods. *Energy* **2017**, *137*, 1286–1292. <https://doi.org/10.1016/j.energy.2017.07.003>.
- (3) van de Bor, D. M.; Infante Ferreira, C. A.; Kiss, A. A. Low Grade Waste Heat Recovery Using Heat Pumps and Power Cycles. *Energy* **2015**, *89*, 864–873. <https://doi.org/10.1016/j.energy.2015.06.030>.
- (4) *Regulation (EU) No 517/2014 of the European Parliament and of the Council of 16 April 2014 on Fluorinated Greenhouse Gases and Repealing Regulation (EC) No 842/2006 Text with EEA Relevance*; 2014; Vol. 150. <http://data.europa.eu/eli/reg/2014/517/oj/eng> (accessed 2023-02-15).
- (5) McLinden, M. O.; Kazakov, A. F.; Steven Brown, J.; Domanski, P. A. A Thermodynamic Analysis of Refrigerants: Possibilities and Tradeoffs for Low-GWP Refrigerants. *Int. J. Refrig.* **2014**, *38*, 80–92. <https://doi.org/10.1016/j.ijrefrig.2013.09.032>.
- (6) Braimakis, K.; Mikelis, A.; Charalampidis, A.; Karella, S. Exergetic Performance of CO₂ and Ultra-Low GWP Refrigerant Mixtures as Working Fluids in ORC for Waste Heat Recovery. *Energy* **2020**, *203*, 117801. <https://doi.org/10.1016/j.energy.2020.117801>.
- (7) Chys, M.; van den Broek, M.; Vanslambrouck, B.; De Paepe, M. Potential of Zeotropic Mixtures as Working Fluids in Organic Rankine Cycles. *Energy* **2012**, *44* (1), 623–632. <https://doi.org/10.1016/j.energy.2012.05.030>.
- (8) Heberle, F.; Preißinger, M.; Brüggemann, D. Zeotropic Mixtures as Working Fluids in Organic Rankine Cycles for Low-Enthalpy Geothermal Resources. *Renew. Energy* **2012**, *37* (1), 364–370. <https://doi.org/10.1016/j.renene.2011.06.044>.
- (9) Pabon, J. J. G.; Khosravi, A.; Belman-Flores, J. M.; Machado, L.; Revellin, R. Applications of Refrigerant R1234yf in Heating, Air Conditioning and Refrigeration Systems: A Decade of Researches. *Int. J. Refrig.* **2020**, *118*, 104–113. <https://doi.org/10.1016/j.ijrefrig.2020.06.014>.
- (10) Dawo, F.; Fleischmann, J.; Kaufmann, F.; Schifflechner, C.; Eyerer, S.; Wieland, C.; Spliethoff, H. R1224yd(Z), R1233zd(E) and R1336mzz(Z) as Replacements for R245fa: Experimental Performance, Interaction with Lubricants and Environmental Impact. *Appl. Energy* **2021**, *288*, 116661. <https://doi.org/10.1016/j.apenergy.2021.116661>.
- (11) Eyerer, S.; Dawo, F.; Kaindl, J.; Wieland, C.; Spliethoff, H. Experimental Investigation of Modern ORC Working Fluids R1224yd(Z) and R1233zd(E) as Replacements for R245fa. *Appl. Energy* **2019**, *240*, 946–963. <https://doi.org/10.1016/j.apenergy.2019.02.086>.
- (12) Yang, J.; Ye, Z.; Yu, B.; Ouyang, H.; Chen, J. Simultaneous Experimental Comparison of Low-GWP Refrigerants as Drop-in Replacements to R245fa for Organic Rankine Cycle Application: R1234ze(Z), R1233zd(E), and R1336mzz(E). *Energy* **2019**, *173*, 721–731. <https://doi.org/10.1016/j.energy.2019.02.054>.
- (13) Jiang, J.; Hu, B.; Wang, R. Z.; Liu, H.; Zhang, Z.; Li, H. Theoretical Performance Assessment of Low-GWP Refrigerant R1233zd(E) Applied in High Temperature Heat Pump System. *Int. J. Refrig.* **2021**, *131*, 897–908. <https://doi.org/10.1016/j.ijrefrig.2021.03.026>.
- (14) Coquelet, C.; Richon, D. Experimental Determination of Phase Diagram and Modeling: Application to Refrigerant Mixtures. *Int. J. Refrig.* **2009**, *32* (7), 1604–1614. <https://doi.org/10.1016/j.ijrefrig.2009.03.013>.
- (15) Abbadi, J. E.; Coquelet, C.; Valtz, A.; Houriez, C. Experimental Measurements and Modelling of Vapour–liquid Equilibria for Four Mixtures of 2,3,3,3-tetrafluoropropene (R1234yf) with 1,1,1,2-tetrafluoroethane (R134a) or 1,1-difluoroethane (R152a) or

- Trans-1-chloro-3,3,3-trifluoropropene (R1233zd(E)) or 2-chloro-3,3,3-trifluoropropene (R1233xf). *Int. J. Refrig.* **2022**, *140*, 172–185. <https://doi.org/10.1016/j.ijrefrig.2022.05.006>.
- (16) Juntarachat, N.; Valtz, A.; Coquelet, C.; Privat, R.; Jaubert, J.-N. Experimental Measurements and Correlation of Vapor–Liquid Equilibrium and Critical Data for the CO₂ + R1234yf and CO₂ + R1234ze(E) Binary Mixtures. *Int. J. Refrig.* **2014**, *47*, 141–152. <https://doi.org/10.1016/j.ijrefrig.2014.09.001>.
- (17) Madani, H.; Valtz, A.; Zhang, F.; El Abbadi, J.; Houriez, C.; Paricaud, P.; Coquelet, C. Isothermal Vapor–Liquid Equilibrium Data for the Trifluoromethane (R23) + 2,3,3,3-Tetrafluoroprop-1-Ene (R1234yf) System at Temperatures from 254 to 348 K. *Fluid Phase Equilibria* **2016**, *415*, 158–165. <https://doi.org/10.1016/j.fluid.2016.02.005>.
- (18) Yang, Z.; Valtz, A.; Coquelet, C.; Wu, J.; Lu, J. Critical Properties and Vapor-Liquid Equilibrium of Two near-Azeotropic Mixtures Containing HFOs. *Int. J. Refrig.* **2022**, *138*, 133–147. <https://doi.org/10.1016/j.ijrefrig.2022.03.027>.
- (19) Teinz, K.; Manuel, S. R.; Chen, B. B.; Pigamo, A.; Doucet, N.; Kemnitz, E. Catalytic Formation of 2,3,3,3-Tetrafluoropropene from 2-Chloro-3,3-Trifluoropropene at Fluorinated Chromia: A Study of Reaction Pathways. *Appl. Catal. B Environ.* **2015**, *165*, 200–208. <https://doi.org/10.1016/j.apcatb.2014.09.076>.
- (20) Mondéjar, M. E.; McLinden, M. O.; Lemmon, E. W. Thermodynamic Properties of Trans-1-Chloro-3,3,3-Trifluoropropene (R1233zd(E)): Vapor Pressure, (p, p, T) Behavior, and Speed of Sound Measurements, and Equation of State. *J. Chem. Eng. Data* **2015**, *60* (8), 2477–2489. <https://doi.org/10.1021/acs.jced.5b00348>.
- (21) Sakoda, N.; Higashi, Y.; Akasaka, R. Measurements of Vapor Pressures for Trans-1-Chloro-3,3,3-Trifluoropropene (R1233zd(E)) and Cis-1,1,1,4,4,4-Hexafluoro-2-Butene (R1336mzz(Z)). *J. Chem. Eng. Data* **2020**, *65* (9), 4285–4289. <https://doi.org/10.1021/acs.jced.0c00239>.
- (22) Di Nicola, G.; Fedele, L.; Brown, J. S.; Bobbo, S.; Coccia, G. Saturated Pressure Measurements of Trans-1-Chloro-3,3,3-Trifluoroprop-1-Ene (R1233zd(E)). *J. Chem. Eng. Data* **2017**, *62* (9), 2496–2500. <https://doi.org/10.1021/acs.jced.6b00916>.
- (23) Brown, J. S.; Coccia, G.; Tomassetti, S.; Pierantozzi, M.; Di Nicola, G. Vapor Phase PvTx Measurements of Binary Blends of Trans-1-Chloro-3,3,3-Trifluoroprop-1-Ene + Isobutane and Cis-1,3,3,3-Tetrafluoroprop-1-Ene + Isobutane. *J. Chem. Eng. Data* **2018**, *63* (1), 169–177. <https://doi.org/10.1021/acs.jced.7b00769>.
- (24) Zhang, W.; Yang, Z.; Lu, J.; Lu, J. Vapor Pressures of 2-Chloro-3,3,3-Trifluoropropene (HCFO-1233xf). *J. Chem. Eng. Data* **2013**, *58* (8), 2307–2310. <https://doi.org/10.1021/je400407z>.
- (25) Yang, Z.; Kou, L.; Lu, J.; Zhang, W.; Mao, W.; Lu, J. Isothermal Vapor–Liquid Equilibria Measurements for Binary Systems of 2,3,3,3-Tetrafluoropropene (HFO-1234yf) + 2-Chloro-3,3,3-Trifluoropropene (HCFO-1233xf) and 2-Chloro-3,3,3-Trifluoropropene (HCFO-1233xf) + 2-Chloro-1,1,1,2-Tetrafluoropropane (HCFC-244bb). *Fluid Phase Equilibria* **2016**, *414*, 143–148. <https://doi.org/10.1016/j.fluid.2016.01.027>.
- (26) Peng, D.-Y.; Robinson, D. B. A New Two-Constant Equation of State. *Ind. Eng. Chem. Fundam.* **1976**, *15* (1), 59–64. <https://doi.org/10.1021/i160057a011>.
- (27) Coquelet, C.; El Abbadi, J.; Houriez, C. Prediction of Thermodynamic Properties of Refrigerant Fluids with a New Three-Parameter Cubic Equation of State. *Int. J. Refrig.* **2016**, *69*, 418–436. <https://doi.org/10.1016/j.ijrefrig.2016.05.017>.
- (28) Mathias, P. M.; Copeman, T. W. Extension of the Peng–Robinson Equation of State to Complex Mixtures: Evaluation of the Various Forms of the Local Composition Concept. *Fluid Phase Equilibria* **1983**, *13*, 91–108. [https://doi.org/10.1016/0378-3812\(83\)80084-3](https://doi.org/10.1016/0378-3812(83)80084-3).

- (29) Laugier, S.; Richon, D. New Apparatus to Perform Fast Determinations of Mixture Vapor–Liquid Equilibria up to 10 MPa and 423 K. *Rev. Sci. Instrum.* **1986**, *57* (3), 469–472. <https://doi.org/10.1063/1.1138909>.
- (30) Peper, S.; Fonseca, J. M. S.; Dohrn, R. High-Pressure Fluid-Phase Equilibria: Trends, Recent Developments, and Systems Investigated (2009–2012). *Fluid Phase Equilibria* **2019**, *484*, 126–224. <https://doi.org/10.1016/j.fluid.2018.10.007>.
- (31) Boonaert, E.; Valtz, A.; Brocuz, J.; Coquelet, C.; Beucher, Y.; De Carlan, F.; Fourmigué, J.-M. Vapor–Liquid Equilibrium Measurements for 5 Binary Mixtures Involving HFO-1336mzz(E) at Temperatures from 313 to 353 K and Pressures up to 2.735 MPa. *Int. J. Refrig.* **2020**, *114*, 210–220. <https://doi.org/10.1016/j.ijrefrig.2020.02.016>.
- (32) Valtz, A.; Abbadi, J. E.; Coquelet, C.; Houriez, C. Experimental Measurements and Modelling of Vapour–Liquid Equilibrium of 2,3,3,3-Tetrafluoropropene (R-1234yf) + 1,1,1,2,2-Pentafluoropropane (R-245cb) System. *Int. J. Refrig.* **2019**, *107*, 315–325. <https://doi.org/10.1016/j.ijrefrig.2019.07.024>.
- (33) Wang, S.; Fauve, R.; Coquelet, C.; Valtz, A.; Houriez, C.; Artola, P.-A.; Ahmar, E. E.; Rousseau, B.; Hu, H. Vapor–Liquid Equilibrium and Molecular Simulation Data for Carbon Dioxide (CO₂) + trans-1,3,3,3-Tetrafluoroprop-1-Ene (R-1234ze(E)) Mixture at Temperatures from 283.32 to 353.02 K and Pressures up to 7.6 MPa. *Int. J. Refrig.* **2019**, *98*, 362–371. <https://doi.org/10.1016/j.ijrefrig.2018.10.032>.
- (34) JCGM. Evaluation of Measurement Data - Guide to the Expression of Uncertainty in Measurement, 2008.
- (35) Taylor, B. N.; Kuyatt, C. E. *Guidelines for Evaluating and Expressing the Uncertainty of NIST Measurement Results*; 2009.
- (36) Guilbot, P.; Valtz, A.; Legendre, H.; Richon, D. Rapid On-Line Sampler-Injector: A Reliable Tool for HT-HP Sampling and on-Line GC Analysis. *Analusis* **2000**, *28* (5), 426–431. <https://doi.org/10.1051/analusis:2000128>.
- (37) Sandler, S. I. *Chemical, Biochemical, and Engineering Thermodynamics*; John Wiley & Sons, 2017.
- (38) Michelsen, M. L.; Mollerup, J. M. *Thermodynamic Models: Fundamentals & Computational Aspects*, 2nd ed.; Tie-Line, 2007.
- (39) Kay, W. B. Pressure–Volume–Temperature Relations for n-Butane. *Ind. Eng. Chem.* **1940**, *32* (3), 358–360. <https://doi.org/10.1021/ie50363a016>.
- (40) Thol, M.; Dubberke, F. H.; Baumhögger, E.; Span, R.; Vrabec, J. Speed of Sound Measurements and a Fundamental Equation of State for Hydrogen Chloride. *J. Chem. Eng. Data* **2018**, *63* (7), 2533–2547. <https://doi.org/10.1021/acs.jced.7b01031>.
- (41) Span, R.; Wagner, W. A New Equation of State for Carbon Dioxide Covering the Fluid Region from the Triple-Point Temperature to 1100 K at Pressures up to 800 MPa. *J. Phys. Chem. Ref. Data* **1996**, *25* (6), 1509. <https://doi.org/10.1063/1.555991>.
- (42) Morrison, G.; Ward, D. K. Thermodynamic Properties of Two Alternative Refrigerants: 1,1-Dichloro-2,2,2-Trifluoroethane (R123) and 1,1,1,2-Tetrafluoroethane (R134a). *Fluid Phase Equilibria* **1991**, *62* (1), 65–86. [https://doi.org/10.1016/0378-3812\(91\)87006-U](https://doi.org/10.1016/0378-3812(91)87006-U).
- (43) Holcomb, C. D.; Niesen, V. G.; Van Poolen, L. J.; Outcalt, S. L. Coexisting Densities, Vapor Pressures and Critical Densities of Refrigerants R-32 and R-152a, at 300–385 K. *Fluid Phase Equilibria* **1993**, *91* (1), 145–157. [https://doi.org/10.1016/0378-3812\(93\)85085-Z](https://doi.org/10.1016/0378-3812(93)85085-Z).
- (44) Tanaka, K. Measurements of Vapor Pressure and Saturated Liquid Density for R245fa. *Trans. Jpn. Soc. Refrig. Air Cond. Eng.* **2014**, *31* (1), 11–17. <https://doi.org/10.11322/tjsrae.31.11>.
- (45) Hulse, R. J.; Basu, R. S.; Singh, R. R.; Thomas, R. H. P. Physical Properties of HCFO-1233zd(E). *J. Chem. Eng. Data* **2012**, *57* (12), 3581–3586. <https://doi.org/10.1021/je300776s>.

- (46) van Konynenburg, P. H.; Scott, R. L.; Rowlinson, J. S. Critical Lines and Phase Equilibria in Binary van Der Waals Mixtures. *Philos. Trans. R. Soc. Lond. Ser. Math. Phys. Sci.* **1997**, *298* (1442), 495–540. <https://doi.org/10.1098/rsta.1980.0266>.

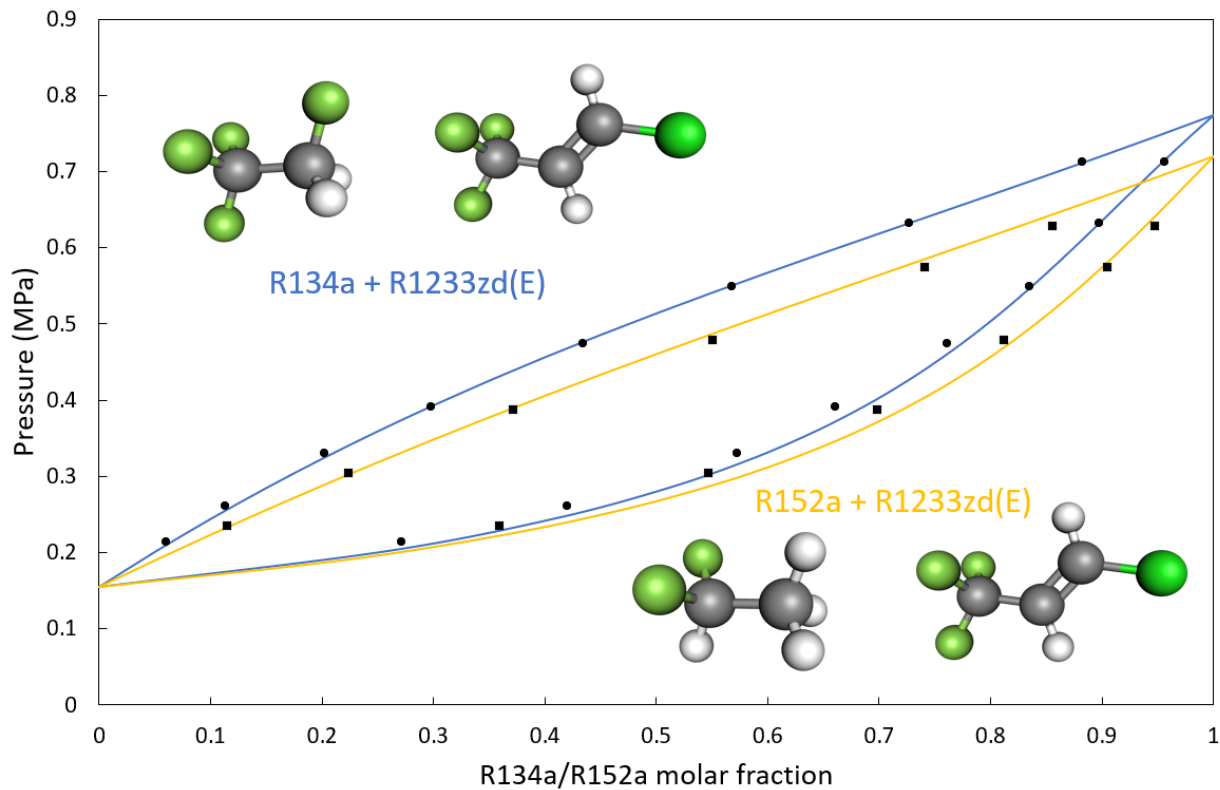


Table of Contents graphic